



Five-phase space vector carrier-based PWM for third harmonic injection

Marc Ramos Friedmann · Alexander Möller · Andreas Binder

Received: 24 November 2023 / Accepted: 16 January 2024 / Published online: 13 March 2024
© The Author(s) 2024

Abstract Five-phase AC drives allow a third harmonic voltage to be fed into the stator winding – in addition to the fundamental voltage – to generate a third harmonic magnetic air gap field. This allows the generation of an additional small constant torque. Furthermore, the undesirable saturation harmonics that occur with saturated iron can be compensated. The desired third harmonic voltage is commonly generated via time-consuming space vector PWM algorithms, which are not well-suited for real-time application, or via look-up tables, which require an increased storage capacity. In our case, the desired third harmonic voltage is generated in the five-phase voltages by adding a non-sinusoidal zero-sequence voltage with five times the fundamental frequency to the fundamental voltage reference signals in carrier-based pulse width modulation (PWM) with a constant switching frequency. This is equivalent to a space vector PWM method (SVPWM) and avoids a significantly high calculation effort. The PWM algorithm programmed in *MATLAB* in real time allows the fast generation of a third harmonic voltage per phase with freely definable amplitude and phase shift without requiring a lot of storage capacity.

Keywords Space vector PWM · Five-phase · Carrier-based PWM · Multiphase · Third harmonic injection

Fünfphasige trägerbasierte Raumzeigermodulation zur Einprägung einer dritten Harmonischen

Zusammenfassung Fünfphasige Drehstromantriebe erlauben es, neben der Spannungsgrundschwingung eine dritte harmonische Oberschwingungsspannung in die Statorwicklung zur Erzeugung einer dritten magnetischen Luftspalt-Feldoberwelle einzuspeisen. Damit kann ein zusätzliches kleines konstantes Drehmoment erzeugt werden. Weiterhin kann damit die bei gesättigtem Eisen auftretende, unerwünschte Sättigungsoberschwingung kompensiert werden. Die gewünschte dritte harmonische Spannung wird üblicherweise über zeitaufwändige Raumzeigermodulations-Algorithmen erzeugt, die für Echtzeitanwendungen nicht gut geeignet sind, oder über Nachschlagetabellen, die eine erhöhte Speicherkapazität erfordern. In unserem Fall wird die gewünschte dritte Spannungsüberschwingung in den fünf Phasenspannungen durch das Hinzufügen einer nichtsinusförmigen Nullspannung mit fünffacher Grundfrequenz zur grundfrequenter Spannungsvorgabe bei der trägerbasierten Pulsweitenmodulation (PWM) mit konstanter Schaltfrequenz erzeugt. Dies entspricht einer PWM mit dem Raumzeigerverfahren (Space Vector-PWM: SVPWM) und vermeidet einen deutlich erhöhten Rechenaufwand. Der in *MATLAB* programmierte PWM-Algorithmus in Echtzeit gestattet die schnelle Erzeugung einer dritten Spannungsüberschwingung je Phase mit frei einstellbarer Amplitude und Phasenlage ohne großen Speicherplatzbedarf.

Schlüsselwörter Raumzeigermodulation · Fünfphasig · Trägerbasierte Modulation · Mehrphasig · Dritte Harmonische-Einprägung

M. Ramos Friedmann · A. Möller (✉) · A. Binder
Institute of Electrical Energy Conversion,
Technical University of Darmstadt,
Landgraf-Georg-Straße 4, 64283 Darmstadt, Germany
amoeller@ew.tu-darmstadt.de

1 Introduction

Although three-phase drives remain the standard in most applications, research on multiphase drives has gained momentum due to their higher efficiency and higher torque-per-volume ratio, compared to their three-phase counterparts [1, 2]. A further factor favouring the use of a phase count bigger than three is the fact that variable speed drives operate with power electronics without restriction of the three phases from the public grid. The additional degree of freedom regarding the voltage generation demands appropriate control and modulation strategies suited for real-time application when operating multiphase drives. This paper focuses on the injection of an arbitrary 3rd harmonic voltage, which allows, for example, to maximise the output torque for induction machines and PM synchronous machines or to compensate saturation harmonics.

The most common strategy for the voltage generation is the Pulse Width Modulation (PWM) of the DC-link voltage. Widely used switching strategies for the power electronics are the continuous carrier-based modulation strategies with (1) a sinusoidal modulation signal [3, 4], (2) Fifth Harmonic Injection (FHI) [3, 4] and (3) Space Vector Modulation (SVM) with its continuous (SVPWM) and discontinuous (DPWM) variants [5–16]. The carrier-based PWM with a reference modulation signal is similar to the three-phase system, where the reference signal (mostly a sine wave function) is compared to a high frequency carrier signal of fixed frequency to determine the switching instants of the ten power electronic switches. To increase the output voltage amplitude and thus improve the DC-link voltage utilisation, [4] expands for multiphase systems the concept of injecting a harmonic signal to the sinusoidal reference signal to achieve a peak reduction of the modulation signals. For three-phase systems, the 3rd harmonic is injected, as it cancels out in the line-to-line voltages and does not lead to additional stator currents in Y-connected windings. For a five-phase system, it is the 5th harmonic that yields the same behaviour. In [3], the method for optimal amplitude and phase of the 5th harmonic component which achieve the largest peak reduction for improved DC voltage utilisation is described.

The SVPWM algorithm in [17] for three-phase systems selects the neighbouring space vectors of a needed reference voltage space vector, which have $2^3 = 8$ discrete values, to approximate, by selected conducting time intervals of the power switches, the reference voltage space vector. In [5–16] strategies implementing neighbouring space vector values of a five-phase system by using different combinations of $2^5 = 32$ discrete space vector values are discussed. The preferred method selects four neighbouring discrete space vector values to nullify an unwanted 3rd harmonic voltage component [5, 7, 11, 12, 18].

Further development on PWM strategies focused on methods to allow a 3rd harmonic voltage in order to generate an additional and constant torque component, as it was mentioned above. Although different in detail, all these described methods [8, 13, 18–23] show rather complex algorithms for the selection of suitable discrete space vector values, the calculation of conduction time intervals of the power switches and lastly the definition of the switching order for minimal switching losses. These steps are computationally time-consuming and thus not well-suited for real-time application. Methods which are in favour for online application follow different approaches, such as the definition of modulation functions based on the calculation of duty cycles [11, 15] or the use of look-up tables by running the algorithm offline and storing the resulting data [18, 20]. However, though faster, the latter solution requires more storage capacity.

Only a few publications, [9, 16] for a five-phase or [24] for a nine-phase system, mention the method of adding the triangle zero-sequence signal as an equivalent of SVPWM, as it is done for three-phase systems. This strategy is faster and simpler to be implemented online and does not require much storage capacity. In [9, 16] the focus is on the peak reduction of the fundamental reference signal for sinusoidal feeding of the drive to improve the utilisation of the DC-link voltage. By injecting an arbitrary 3rd harmonic component in addition to the fundamental component, our contribution expands the idea by adding a non-sinusoidal zero-sequence signal for an additional injection of an arbitrary 3rd harmonic component.

Sect. 2 briefly describes the concept of three-phase space vector modulation and its equivalence to the addition of a 3rd harmonic triangle zero-sequence signal. Sect. 3 defines the five-phase voltage reference signals, used as input for the considered algorithm. Sect. 4 describes the differences and challenges of five-phase space vector PWM compared to a three-phase system, and introduces the SVPWM algorithm in [18]. Sect. 5 explains how the modulation signals are generated for the carrier-based PWM, based on the addition of a non-sinusoidal zero-sequence signal, and for the SVPWM algorithm of [18] with *MATLAB*. Sect. 6 compares the resulting modulation signals of both modulation schemes for three different examples and performs a Fast Fourier Transform (FFT) analysis on the zero-sequence signals.

2 Three-phase space vector modulation

The concept of SVM [17] is based on the fact that the switching combinations of a three-phase inverter can be considered to be discrete space vectors in the $\alpha\beta$ plane gained by applying *Clarke's* transformation matrix. With $2^3 = 8$ possible combinations, the $\alpha\beta$ plane is divided into six sectors by six active discrete

space vectors, which are separated by $\frac{360^\circ}{2 \cdot 3} = 60^\circ$, respectively. The remaining two switching combinations are associated with zero space vectors (either all three upper or lower power switches are conducting) giving eight different discrete space vector values.

The needed reference voltage space vector is used as input. First, the sector in which the reference space vector is located, is identified. From that, the two active discrete space vectors neighbouring that sector are determined. The conduction time intervals t_1 and t_2 of the power switches for both space vectors are calculated to approximate the reference space vector. If the sum $t_1 + t_2$ is smaller than the predefined sampling period T_s , the remaining time $t_0 = T_s - (t_1 + t_2)$ is used for operating the zero space vectors. The allocation of t_0 to each of the two zero space vectors is the "degree of freedom", resulting from SVM, from which different modulation schemes arise. These schemes divided into groups are a) the continuous symmetrical SVPWM and b) the discontinuous DPWM. In both cases, the algorithm is computationally time-consuming and not well-suited for real-time applications. Hence, [25] introduced the idea of an equivalent modulation scheme, based on carrier-based PWM, where a triangle zero-sequence signal

$$u_0 = -\frac{1}{2} \cdot (u_{\text{ref,max}} + u_{\text{ref,min}}) \tag{1}$$

is added to the reference phase voltage signals $u_{\text{ref,U}}$, $u_{\text{ref,V}}$ and $u_{\text{ref,W}}$, where $u_{\text{ref,max}} = \max(u_{\text{ref,U}}, u_{\text{ref,V}}, u_{\text{ref,W}})$ and $u_{\text{ref,min}} = \min(u_{\text{ref,U}}, u_{\text{ref,V}}, u_{\text{ref,W}})$, holds, in order to determine the modulation signals

$$u_{\text{mod},x} = u_{\text{ref},x} + u_0 \quad \text{for } x = \text{U, V and W.} \tag{2}$$

The zero-sequence u_0 signal has a frequency three times higher than the fundamental frequency f_1 and does not have any impact on the line-to-line voltages as it cancels out according to $u_{\text{mod,U}} - u_{\text{mod,V}} = u_{\text{ref,U}} - u_{\text{ref,V}} + u_0 - u_0$. This solution is a good alternative due to its simplicity and fast implementation and is used in the following for five-phase drives.

3 Reference signals

For a five-phase drive ($m = 5$), according to (2), five reference signals $u_{\text{ref},x}$ are introduced per phase:

$$u_{\text{ref},x} = m_{a,1} \cdot \cos\left(\omega_1 t - n_x \cdot \frac{2\pi}{5}\right) + m_{a,3} \cdot \cos\left(3 \cdot \omega_1 t - 3 \cdot n_x \cdot \frac{2\pi}{5} - \varphi_3\right). \tag{3a}$$

$$x = \text{a, b, c, d, e (five phases)} \tag{3b}$$

$$n_x : n_a = 0, n_b = 1, n_c = 2, n_d = 3, n_e = 4. \tag{3c}$$

In (3), the electric fundamental angular frequency is $\omega_1 = 2\pi \cdot f_1$, and $3\omega_1$ constitutes the 3rd harmonic. Both ω_1 - and $3\omega_1$ -voltage components form a sym-

metrical five-phase system in (3), where the phases are phase-shifted to each other either by $\frac{2\pi}{5}$ or $3 \cdot \frac{2\pi}{5}$ respectively to generate either the fundamental or the 3rd harmonic voltage component. The 3rd harmonic component is phase-shifted with respect to the fundamental component by φ_3 . The amplitudes of both reference components are described by the amplitude modulation ratios $m_{a,1}$ and $m_{a,3}$, which refer the sinusoidal reference phase voltage amplitudes $\hat{U}_{\text{ref},1}$ and $\hat{U}_{\text{ref},3}$ to half the DC-link voltage $\frac{U_{\text{DC}}}{2}$ (4). Therefore, the reference and modulation signals are given in p.u.

$$m_{a,i} = \frac{\hat{U}_{\text{ref},i}}{U_{\text{DC}}/2} \quad \text{with } i = 1 \text{ and } 3. \tag{4}$$

4 Five-phase space vector modulation

Fig. 1 shows the circuit for a five-phase two-level Voltage Source Inverter (VSI) where the upper power switches in each phase leg are represented by ideal switches and given boolean variables S_a, \dots, S_e . These adopt only "1" (switch ON) or "0" (switch OFF) as values. We assume ideal switching, thus the lower power switches in each phase leg represent the negative logic of the respective upper power switches $\bar{S}_a, \dots, \bar{S}_e$. Therefore only the five upper switches are considered. In [12, 14], the phase voltages $u_{x,n}$, where $x = \text{a, b, c, d, e}$ (five phases), are defined as in (5).

$$u_{an} = U_{\text{DC}} \cdot \left(\frac{4}{5} \cdot S_a - \frac{1}{5} \cdot (S_b + S_c + S_d + S_e) \right) \tag{5a}$$

$$u_{bn} = U_{\text{DC}} \cdot \left(\frac{4}{5} \cdot S_b - \frac{1}{5} \cdot (S_a + S_c + S_d + S_e) \right) \tag{5b}$$

$$u_{cn} = U_{\text{DC}} \cdot \left(\frac{4}{5} \cdot S_c - \frac{1}{5} \cdot (S_a + S_b + S_d + S_e) \right) \tag{5c}$$

$$u_{dn} = U_{\text{DC}} \cdot \left(\frac{4}{5} \cdot S_d - \frac{1}{5} \cdot (S_a + S_b + S_c + S_e) \right) \tag{5d}$$

$$u_{en} = U_{\text{DC}} \cdot \left(\frac{4}{5} \cdot S_e - \frac{1}{5} \cdot (S_a + S_b + S_c + S_d) \right) \tag{5e}$$

[12, 14] transform the phase voltages in (5) into the $\alpha\beta_1$ - and $\alpha\beta_3$ -planes with a matrix similar to Clarke's

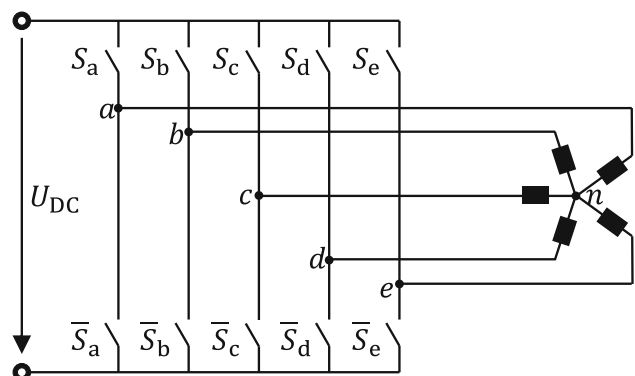


Fig. 1 Five-phase two-level voltage source inverter (VSI) with ideal switches

transformation matrix adapted to five-phase systems (6).

$$\begin{bmatrix} u_{\alpha 1} \\ u_{\beta 1} \\ u_{\alpha 3} \\ u_{\beta 3} \\ u_0 \end{bmatrix} = \frac{2}{5} \begin{bmatrix} 1 & \cos\left(\frac{2\pi}{5}\right) & \cos\left(\frac{4\pi}{5}\right) & \cos\left(\frac{6\pi}{5}\right) & \cos\left(\frac{8\pi}{5}\right) \\ 0 & \sin\left(\frac{2\pi}{5}\right) & \sin\left(\frac{4\pi}{5}\right) & \sin\left(\frac{6\pi}{5}\right) & \sin\left(\frac{8\pi}{5}\right) \\ 1 & \cos\left(\frac{6\pi}{5}\right) & \cos\left(\frac{12\pi}{5}\right) & \cos\left(\frac{18\pi}{5}\right) & \cos\left(\frac{24\pi}{5}\right) \\ 0 & \sin\left(\frac{6\pi}{5}\right) & \sin\left(\frac{12\pi}{5}\right) & \sin\left(\frac{18\pi}{5}\right) & \sin\left(\frac{24\pi}{5}\right) \\ \frac{1}{2} & \frac{1}{2} & \frac{1}{2} & \frac{1}{2} & \frac{1}{2} \end{bmatrix} \begin{bmatrix} u_{an} \\ u_{bn} \\ u_{cn} \\ u_{dn} \\ u_{en} \end{bmatrix} \quad (6)$$

The five upper power switches in the VSI (Fig. 1) have $2^5 = 32$ different possible switching combinations. Each of the 32 switching combinations is inserted in (5) and mapped onto the $\alpha\beta_1$ - and $\alpha\beta_3$ -planes with (6). This results in 30 different active discrete space vectors and two zero space vectors. The active space vectors divide the $\alpha\beta_1$ -plane for the ω_1 -voltage in ten sectors, with each sector covering an angle of $\frac{360^\circ}{2 \cdot 5} = 36^\circ$. Consequently, each sector has three neighbouring discrete space vectors on each side (Fig. 2a). These three active discrete space vectors per side are classified into three different categories

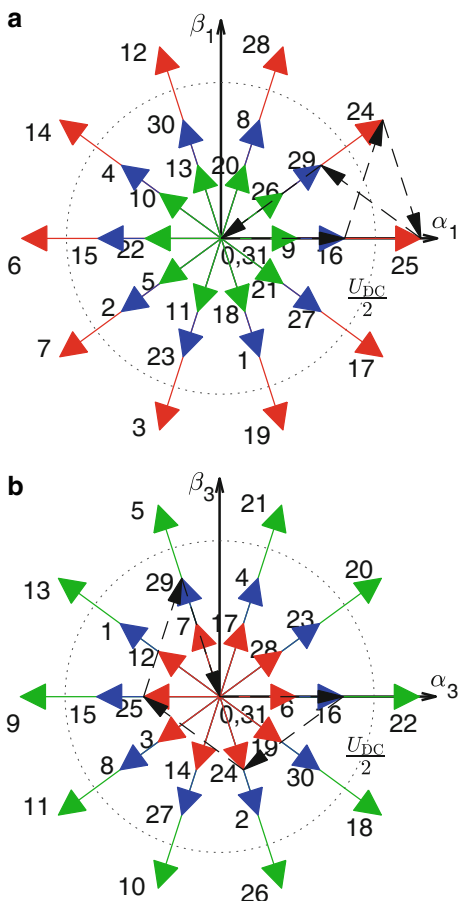


Fig. 2 Resulting 32 discrete space vectors for each five-phase inverter switching combination projecting **a** the fundamental components onto the $\alpha\beta_1$ plane and **b** the 3rd harmonic components onto the $\alpha\beta_3$ plane. The dashed black arrows show the switching sequence for a sector within a sampling period T_s for the SVPWM algorithm based on neighbouring space vectors (similar to [12])

S, M, L based on their magnitudes: Small, Medium and Large ($S / M / L$) ($0.25 \cdot U_{DC} / 0.40 \cdot U_{DC} / 0.65 \cdot U_{DC}$). It is needed to consider a second $\alpha\beta_3$ -plane (Fig. 2b) where the space vectors for the 3rd harmonic reference components are located. This second plane also contains all 30 active discrete space vectors, but they are located in different sectors with respect to their counterparts in the $\alpha\beta_1$ -plane. The large vectors (*L*) in the $\alpha\beta_1$ -plane become small (*S*) in the $\alpha\beta_3$ -plane and the small vectors (*S*) in the $\alpha\beta_1$ -plane become large (*L*) in the $\alpha\beta_3$ -plane (Fig. 2b). For example, the discrete voltage space vector $25_{10} = 11001_2$ results from the switching combination $S_a = 1, S_b = 1, S_c = 0, S_d = 0$ and $S_e = 1$. The phase voltages thus result in $u_{an} = 0.4 \cdot U_{DC}, u_{bn} = 0.4 \cdot U_{DC}, u_{cn} = -0.6 \cdot U_{DC}, u_{dn} = -0.6 \cdot U_{DC}$ and $u_{en} = 0.4 \cdot U_{DC}$, and mapped onto the $\alpha\beta_1$ - and $\alpha\beta_3$ -planes: $u_{\alpha 1} = 0.65 \cdot U_{DC}, u_{\beta 1} = 0, u_{\alpha 3} = -0.25 \cdot U_{DC}, u_{\beta 3} = 0$ and $u_0 = 0$ (Fig. 2).

4.1 Five-phase space vector PWM algorithm with neighbouring vectors

First, it must be decided how many and which of the neighbouring space vectors are required for approximating the reference space vector. As the discrete space vectors are present in both $\alpha\beta_1$ - and $\alpha\beta_3$ -planes simultaneously, the generation of a ω_1 -voltage reference space vector leads to the inevitable creation of a 3rd harmonic [5, 7, 11, 12, 18]. If for example the two largest vectors (*L*) per sector in the $\alpha\beta_1$ -plane are selected to generate a fundamental voltage space vector, a small 3rd harmonic voltage space vector is created in the $\alpha\beta_3$ -plane. Therefore [5, 7, 11, 12, 18] concluded that choosing only four neighbouring space vectors in the $\alpha\beta_1$ -plane is a good solution, especially large (*L*) and medium (*M*), in order to nullify the 3rd harmonic voltage space vector. The SVPWM scheme implementing neighbouring large (*L*) and medium (*M*) space vectors in the $\alpha\beta_1$ -plane is therefore the most commonly used strategy. Not using the small space vectors in the $\alpha\beta_1$ -plane is justified by realising that these would produce very large 3rd harmonic voltage components, which are unwanted if the purely feeding of a fundamental voltage component is the objective. Therefore, the algorithm runs as follows: detection of the sector, selection of neighbouring discrete space vectors and calculation of conduction time intervals t_1, t_2, t_3 and t_4 . In our case, the injection of a 3rd harmonic component is also of interest. Therefore, Fig. 3 displays the regions of possible combinations of $m_{a,1}$ and $m_{a,3}$ which are possible with the SVPWM, based on neighbouring large (*L*) and medium (*M*) discrete space vectors. The regions in Fig. 3 were generated by running the previously described algorithm in *MATLAB* for each point in the grid defined by $\varphi_3 = 0 : \frac{\pi}{20} : \pi, m_{a,1} = 0 : 0.001 : 1.25$ and $m_{a,3} = 0 : 0.001 : 1.25$. If the resulting conduction time intervals t_1, t_2, t_3 and t_4 satisfied the conditions $t_1 \geq 0, t_2 \geq 0, t_3 \geq 0, t_4 \geq 0$ and $t_1 + t_2 + t_3 + t_4 \leq T_s$, the respec-

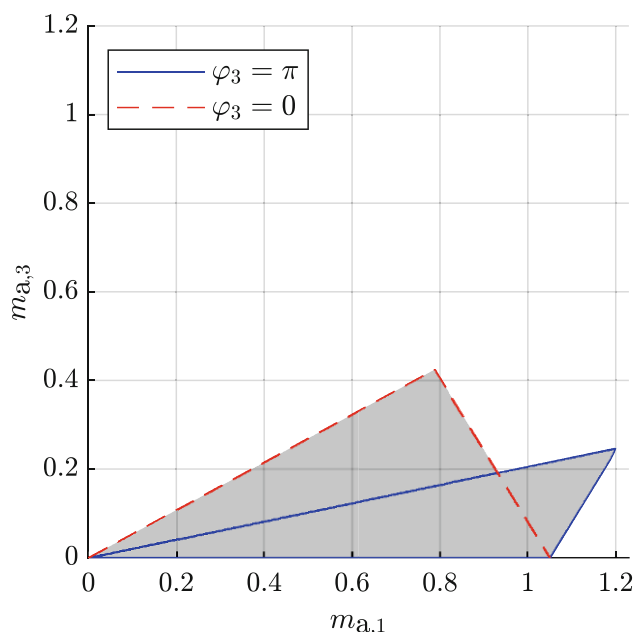


Fig. 3 Simulation of the regions of possible combinations of $m_{a,1}$ and $m_{a,3}$ for the SVPWM algorithm implementing two medium (M) and two large (L) neighbouring space vectors with *MATLAB*

tive ($\varphi_3, m_{a,1}, m_{a,3}$)-values were stored. When the 3rd harmonic is nullified ($m_{a,3} = 0$), the maximum amplitude for the fundamental results in $m_{a,1,\max} = 1.05$. In Fig. 3 it can also be seen that a 3rd harmonic component can only be injected in addition to the fundamental component if it is either in phase ($\varphi_3 = 0^\circ$) or phase opposition ($\varphi_3 = 180^\circ$). This is due to the fact that if $\varphi_3 \neq 0^\circ$ or 180° , the 3rd harmonic space vector component would not lie in the same sector determined by the fundamental component.

4.2 Five-phase space vector PWM algorithms

To overcome the limits for the $3\omega_1$ -component of Fig. 3, new algorithms which are not limited to choosing only neighbouring space vectors have been developed such as in [18]. This leads to the results in Fig. 4. The implementation of the algorithm of [18] demands more computational effort and is therefore not well-suited for real-time applications. It searches a combination of four suitable discrete space vectors, based on their linear independence, and then calculates the conduction time intervals, which have to fulfill the following conditions: $t_1 \geq 0, t_2 \geq 0, t_3 \geq 0, t_4 \geq 0$ and $t_1 + t_2 + t_3 + t_4 \leq T_s$. In addition to that, the algorithm selects the order of the applied active space vectors in order to minimise the number of switching events. To speed up the implementation of the algorithm, it is solved offline and the results are stored into look-up tables. The gain in speed comes at a cost of increased storage space requirement.

5 Generating the modulation signals

Contrary to Sect. 4.2, the addition of a non-sinusoidal zero-sequence signal, with five times the fundamental frequency, is fast and easy to implement and does not require large amounts of storage capacity. In order to compare the carrier-based PWM, based on the addition of a zero-sequence signal, with the SVPWM algorithm of Sect. 4.2, the modulation signals similar to Sect. 2 are generated for each scheme.

5.1 Carrier-based PWM with zero-sequence signal

The modulation signals for the carrier-based PWM are generated similarly to (2) by adding the zero-sequence signal

$$u_0 = -\frac{1}{2} \cdot (u_{\text{ref,max}} + u_{\text{ref,min}}), \quad (7)$$

with $u_{\text{ref,max}} = \max(u_{\text{ref,a}}, u_{\text{ref,b}}, u_{\text{ref,c}}, u_{\text{ref,d}}, u_{\text{ref,e}})$ and $u_{\text{ref,min}} = \min(u_{\text{ref,a}}, u_{\text{ref,b}}, u_{\text{ref,c}}, u_{\text{ref,d}}, u_{\text{ref,e}})$, to all five reference signals in (3).

5.2 Generalised SVPWM algorithm

To generate the modulation signals for the generalised SVPWM algorithm from [18], the algorithm was coded with *MATLAB*. The algorithm first needs a reference vector with four components, which are the components of the reference voltage vectors in the $\alpha\beta_1$ - and $\alpha\beta_3$ -planes, projected onto the four axis $\alpha_1, \beta_1, \alpha_3$ and β_3 :

$$\vec{U}_{\text{ref}} = [u_{\text{ref},\alpha_1} \quad u_{\text{ref},\beta_1} \quad u_{\text{ref},\alpha_3} \quad u_{\text{ref},\beta_3}]^T. \quad (8)$$

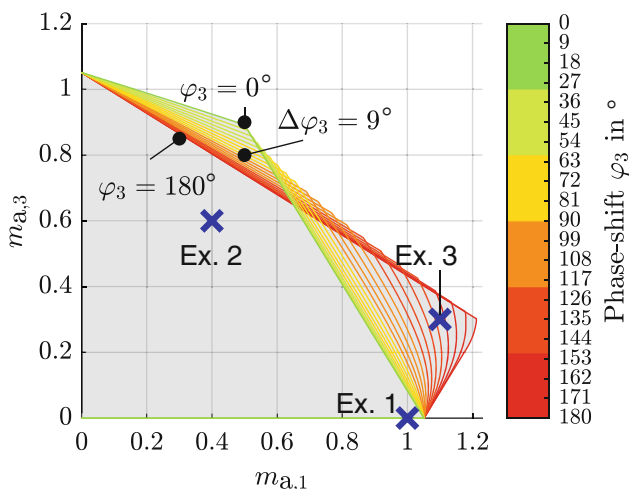


Fig. 4 Simulation of the regions of possible combinations of $m_{a,1}$ and $m_{a,3}$ with *MATLAB* for the carrier-based PWM method which is equivalent to the general SVPWM algorithm from Sect. 5.2 (Ex.: example, see Sect. 6)

5.2.1 Selection criteria

The selection parameter

$$P_i = \frac{\vec{U}_{\text{ref}} \cdot \vec{U}_{\text{fix},i}}{|\vec{U}_{\text{fix},i}|^q} \quad \text{with } i = 1, 2, \dots, 30; \quad q = 2 \quad (9)$$

is calculated for each of the 30 discrete active space vectors

$$\vec{U}_{\text{fix},i} = [u_{\text{fix},i,\alpha1} \quad u_{\text{fix},i,\beta1} \quad u_{\text{fix},i,\alpha3} \quad u_{\text{fix},i,\beta3}]^T \quad (10)$$

and arranged in descending order. The magnitude of the discrete active space vectors $\vec{U}_{\text{fix},i}$ in the denominator of (9) is increased by the exponent $q=2$ in order to prioritise the smaller vectors. Once the list of 30 P_i -values is sorted accordingly, it is used to find the four best suited discrete space vectors $U_{\text{fix},j}$, $U_{\text{fix},k}$, $U_{\text{fix},l}$ and $U_{\text{fix},m}$ where j , k , l and m are the numbers of the selected active discrete space vectors, $1 \leq j, k, l, m \leq 30$. The four selected discrete space vectors must be linear independent from each other. The algorithm iterates through all the elements $P_i(x)$ of the sorted list P_i , starting with the first four elements ($P_j(1)$, $P_k(2)$, $P_l(3)$, $P_m(4)$), where $x = 1, \dots, 30$ is a variable element in the P_i -list. The algorithm takes the discrete space vectors related to the individual elements $P_i(x)$ and tests their linear dependence. First, the linear dependence of the discrete space vectors of $P_j(1)$ and $P_k(2)$ is tested. If linear dependence exists, $P_k(2)$ is ignored and $P_k(3)$ is tested together with $P_j(1)$. If $P_k(x)$ iterates through all the values of the list, the whole process starts again with $P_j(2)$ and $P_k(3)$. This process is repeated, until a linear independent pair of $U_{\text{fix},j}$ and $U_{\text{fix},k}$ is found. Next, a third discrete space vector $U_{\text{fix},l}$ ($P_l(x)$) is selected to test the linear dependence of all three discrete space vectors. The first candidate of $P_l(x)$ belongs to the P_i -value, following the selected $P_k(x)$ value. If linear dependence exists, then the next $P_l(x)$ element is tested. If again all remaining $P_l(x)$ values have been tested without proving linear independence, the next suitable ($P_j(x)$, $P_k(x)$) pair is selected and the search for $P_l(x)$ starts again. The same process is followed to find the fourth discrete space vector $U_{\text{fix},m}$ ($P_m(x)$). If the input reference vector U_{ref} can be realised, the algorithm delivers four linearly independent discrete space vectors $U_{\text{fix},j}$, $U_{\text{fix},k}$, $U_{\text{fix},l}$ and $U_{\text{fix},m}$.

5.2.2 Calculation of the conducting time intervals

The four selected discrete space vectors are arranged as a matrix which is used to calculate the conducting time intervals t_1 , t_2 , t_3 and t_4 of the power switches in (11).

$$\begin{bmatrix} t_1 \\ t_2 \\ t_3 \\ t_4 \end{bmatrix} = T_s \cdot \begin{bmatrix} \vec{U}_{\text{fix},j} & \vec{U}_{\text{fix},k} & \vec{U}_{\text{fix},l} & \vec{U}_{\text{fix},m} \end{bmatrix}^{-1} \cdot \vec{U}_{\text{ref}} \quad (11)$$

If the result of (11) satisfies $t_1 \geq 0$, $t_2 \geq 0$, $t_3 \geq 0$, $t_4 \geq 0$ and $t_1 + t_2 + t_3 + t_4 \leq T_s$, the search is stopped, but if one of the conditions is not held, the iterative search in Sect. 5.2.1 continues with a new set of discrete space vectors.

5.2.3 Switching frequency

When four suitable space vectors have been selected, the next step is to determine their switching order, together with both zero space vectors $U_{\text{fix},0}$ and $U_{\text{fix},31}$. The sequence of these space vectors is determined by the order with the least amount of switching events. The algorithm of [18] no longer ensures that each inverter phase leg switches only once per switching cycle T_s . Therefore the switching frequency f_{sw} is not constant and the switching pattern is not equal for all five phase legs. Thus, [18] calculates a mean switching frequency \bar{f}_{sw} for every possible permutation of switching sequences. The permutation with the lowest average switching frequency is selected. For this calculation a whole period of the fundamental output voltage $T_1 = \frac{1}{f_1}$ is considered, thus increasing the calculation effort. Therefore, we focus on the number of switching events within one switching period T_s .

5.2.4 Determination of the switching sequence

At this point, the selected active discrete space vectors $U_{\text{fix},j}$, $U_{\text{fix},k}$, $U_{\text{fix},l}$, $U_{\text{fix},m}$ and $U_{\text{fix},0}$ and $U_{\text{fix},31}$ are represented by their number ($j, k, l, m, 0, 31$) via a 5 bit binary number. Each bit of the number is assigned to one of the five phase legs. A digit "1" represents the upper switch of a phase leg being "on", and "0" represents that same switch being "off". For example, for $25_{10} = 11001_2$, going from left to right, phases a, b, c, d and e are "on", "on", "off", "off" and "on", respectively. With this information, all $6! = 720$ permutations of the six available discrete space vectors are tested. The test consists of counting for each combination the amount of switching state changes "1→0" and "0→1", in each of the five phase legs ($z_{\text{sw},a}$, $z_{\text{sw},b}$, $z_{\text{sw},c}$, $z_{\text{sw},d}$, $z_{\text{sw},e}$). For this, "switching vectors" S_a, \dots, S_e for each phase leg are defined. For example, for the switching sequence shown in Fig. 2, which is described by $0_{10} = 00000_2 \rightarrow 16_{10} = 10000_2 \rightarrow 24_{10} = 11000_2 \rightarrow 25_{10} = 11001_2 \rightarrow 29_{10} = 11101_2 \rightarrow 31_{10} = 11111_2$, the switching vectors for each phase leg a, ..., e result in

$$\vec{S}_a = [0 \quad 1 \quad 1 \quad 1 \quad 1 \quad 1]^T \rightarrow z_{\text{sw},a} = 1 \quad (12)$$

$$\vec{S}_b = [0 \quad 0 \quad 1 \quad 1 \quad 1 \quad 1]^T \rightarrow z_{\text{sw},b} = 1 \quad (13)$$

$$\vec{S}_c = [0 \quad 0 \quad 0 \quad 0 \quad 1 \quad 1]^T \rightarrow z_{\text{sw},c} = 1 \quad (14)$$

$$\vec{S}_d = [0 \quad 0 \quad 0 \quad 0 \quad 0 \quad 1]^T \rightarrow z_{\text{sw},d} = 1 \quad (15)$$

$$\vec{S}_e = [0 \quad 0 \quad 0 \quad 1 \quad 1 \quad 1]^T \rightarrow z_{\text{sw},e} = 1. \quad (16)$$

The mean value of switching instances \bar{z} for all five phase legs is computed with

$$\bar{z} = \frac{z_{\text{sw},a} + z_{\text{sw},b} + z_{\text{sw},c} + z_{\text{sw},d} + z_{\text{sw},e}}{5} \quad (17)$$

and the permutation with the lowest value is selected. For the switching sequence (0 → 16 → 24 → 25 → 29 → 31) acc. to (12–16), each phase leg has one single switching state change “0 → 1”. The mean value of switching instances results therefore in $\bar{z} = \frac{5 \cdot 1}{5} = 1$.

5.2.5 Generation of the modulation signals

As described in Sect. 4.2, the SVPWM algorithm does not utilise modulation signals. However, for the comparison to the proposed carrier-based PWM, these modulation signals have to be computed from the SVPWM algorithm. These modulation signals are generated via the duty cycles similar to [11]. The algorithm always puts the zero space vectors at the beginning and end of the switching cycles, which leads to an active time vector for the conducting states

$$\vec{t} = \left[\frac{t_0}{2} \quad t_1 \quad t_2 \quad t_3 \quad t_4 \quad \frac{t_0}{2} \right]^T, \quad (18)$$

which contains the active time for the zero space vectors (19).

$$t_0 = T_s - \sum_{i=1}^4 t_i \quad (19)$$

In (18) this time t_0 is the first and last elements of \vec{t} ; hence the sorted “active times” for the active voltage space vectors lie in between. To compute the duty cycles for each phase leg D_a, \dots, D_e , the switching vectors S_a, \dots, S_e are multiplied with the time vector t via scalar vector product (20).

$$D_x = \vec{t} \cdot \vec{S}_x \quad (20a)$$

$$x = a, b, c, d, e \text{ (five phases).} \quad (20b)$$

5.3 Possible combinations of $m_{a,1}$ and $m_{a,3}$

The range of possible combinations of $m_{a,1}$ and $m_{a,3}$ is shown in Fig. 4. The regions in Fig. 4 were generated similarly to Fig. 3 with MATLAB. First, the same grid defined in Sect. 4.1 was defined: $\varphi_3 = 0 : \frac{\pi}{20} : \pi$, $m_{a,1} = 0 : 0.001 : 1.25$ and $m_{a,3} = 0 : 0.001 : 1.25$. The modulation signals defined in Sect. 5.1 were generated for each point in the grid and only when these were ≥ -1 and ≤ 1 for a whole fundamental electric period T_1 , the $(\varphi_3, m_{a,1}, m_{a,3})$ -values were stored. The process was also conducted with the algorithm from Sect. 5.2, where the $(\varphi_3, m_{a,1}, m_{a,3})$ -values were stored whenever the resulting conduction time intervals t_1, t_2, t_3 and t_4 satisfied the conditions $t_1 \geq 0, t_2 \geq 0, t_3 \geq 0, t_4 \geq 0$ and $t_1 + t_2 + t_3 + t_4 \leq T_s$. The resulting regions for both algorithms, described in Sects. 5.1 and 5.2, were identical. For comparative reasons, the range of possible combinations of $m_{a,1}$ and $m_{a,3}$ for carrier-based PWM without zero-sequence signal addition is shown in Fig. 5. The regions in Fig. 5 were generated in the same manner as the regions in Fig. 4. When no

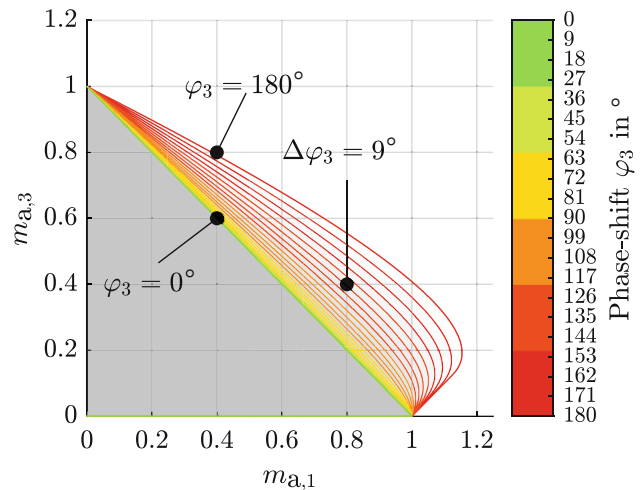


Fig. 5 Simulation of the regions of possible combinations of $m_{a,1}$ and $m_{a,3}$ with MATLAB for the carrier-based PWM method without zero-sequence signal addition

zero-sequence is added, the reference signals in (3) directly become the modulation signals. Obviously the region of possible combinations of $m_{a,1}$ and $m_{a,3}$ for the SVPWM algorithm in [18] is larger than for the algorithm with neighbouring space vectors (Fig. 3). It allows also more combinations of $m_{a,1}$ and $m_{a,3}$ than the method where no zero-sequence is added to the reference signals. This proves that the zero-sequence signal addition allows a peak reduction for a broader range of modulation. The regions of possible combinations of $m_{a,1}$ and $m_{a,3}$ in Figs. 4 and 5 shift their limits in dependence of the chosen phase-shift φ_3 . The region shared by all possible $0^\circ \leq |\varphi_3| \leq 180^\circ$ in Fig. 4 coincides with the ones shown in [22, 23]. The addition of a 3rd harmonic component becomes interesting for the operation of five-phase electric AC motors. Since five-phase motors can generate a 3rd harmonic magnetic air gap field in addition to the fundamental field, the 3rd harmonic voltage can be used to generate this field component. Due to its small magnetizing inductance the torque generation through the 3rd harmonic field yields higher losses and is not recommended at small loads. At high loads and saturation the 3rd harmonic field component increases the efficiency and the output torque. The 3rd harmonic voltage that is required for such operation typically requires the combinations of $m_{a,1}$ and $m_{a,3}$ in Fig. 4 fulfilling the condition $m_{a,3} \lesssim 0.25 \cdot m_{a,1}$ with $m_{a,1} \in [0, 1.05]$ to be possible for any value of φ_3 . Furthermore, in the field weakening range, it is possible, depending on the choice of $m_{a,3} > 0$ and φ_3 , to increase the range of the applicable fundamental voltage $u_{s,1}$ past $m_{a,1} = 1.05$ up to $m_{a,1} \approx 1.21$.

6 Comparing the carrier-based PWM and SVPWM algorithms

In order to show the identical results in the signal shape for the modulation signals of the carrier-based PWM with non-sinusoidal zero-sequence signal addition (method A) and the SVPWM algorithm of [18] (method B) for an arbitrary 3rd harmonic voltage injection, three possible combinations of $m_{a,1}$ and $m_{a,3}$ from Fig. 4 are compared in the examples 1, 2, 3.

- example 1: $m_{a,1} = 1, \quad m_{a,3} = 0, \quad \varphi_3 = 0^\circ$.
 example 2: $m_{a,1} = 0.4, \quad m_{a,3} = 0.6, \quad \varphi_3 = 30^\circ$.
 example 3: $m_{a,1} = 1.1, \quad m_{a,3} = 0.3, \quad \varphi_3 = 153^\circ$.

Example 1 represents the pure sinusoidal feeding with ω_1 . Only the fundamental is injected, and the zero-sequence signal has the well-known shape of a triangle signal. The comparison of both – identical in shape – modulation signals for methods A and B is given in Fig. 6. Example 2 shows a case which acc. to Fig. 4 is possible for all values of φ_3 ($0^\circ \leq |\varphi_3| \leq 180^\circ$), where the 3rd harmonic voltage has a bigger amplitude than the fundamental voltage (Fig. 7). Example 3 is only possible for phase-shift values $144^\circ < |\varphi_3| < 180^\circ$. The resulting identical modulation signals are compared in Fig. 8.

6.1 Comparison of the modulation signals

From Fig. 6–8 it becomes apparent that the wave forms of the modulation signals for methods A and B are the same. The only difference is the scaling on the ordinate and an offset of 0.5. The modulation signals resulting directly from SVPWM [18] have values between 0 to 1 because they are defined by the duty cycles in (20), which are the sum of the computed “active times”. Since the values for t_0, \dots, t_4 cannot be negative, the resulting duty cycles and modulation signals are also positive. If the offset of 0.5 is subtracted from the modulation signals, resulting from method B, and afterwards multiplied by 2, the identical modulation signals, gained from the addition of the non-sinusoidal zero-sequence signal, are obtained. Given that the modulation signals for methods A and B are equal, it also becomes apparent why method A is preferred due to it being better suited for real-time application and not requiring large amounts of storage. Contrary to the proposition in [18], method A does not require the storage of large look-up tables. With respect to the reduced calculation time, method A only requires simple addition, multiplication and logical comparison operations compared to the many tasks present in method B: calculation of 30 P_i values, sorting these, repeatedly iterating through these, calculating the conducting time intervals and determining the switching sequence.

6.2 Analysis of the zero-sequence signals

As stated before, the addition of the zero-sequence signal (7) does not have an effect on the line-to-line voltages and does not produce additional stator currents in the five-phase Y-connected windings. In a five-phase system, the harmonic voltage components $n=5, 10, 15, \dots$ fulfill these conditions. To demonstrate this, an FFT analysis is performed on the resulting zero-sequence signals for examples 1, 2 and 3, to confirm that these only contain harmonics that are a multiple of five. As mentioned in [16] and shown by FFT analysis in Fig. 9a, the zero-sequence signal for pure sinusoidal feeding, shown in Fig. 6a, consists of the 5th, 15th, etc. harmonics. For the other two examples in Figs. 7a and 8a, the signal wave form deviates from the triangle. However, the FFT analysis, shown in Fig. 9b and c respectively, shows simila

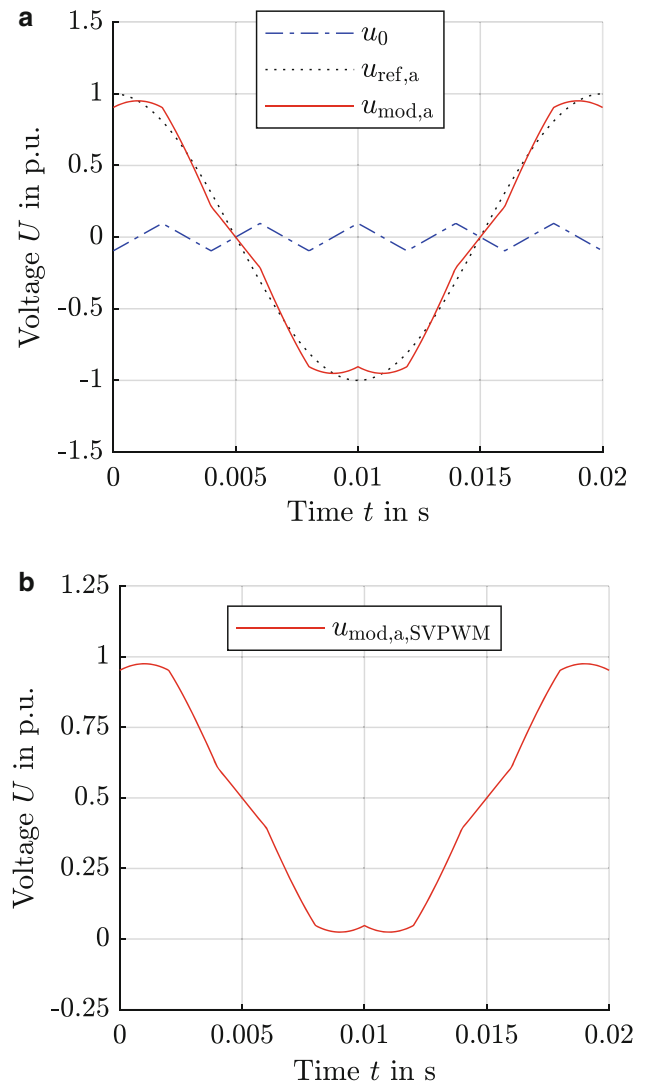


Fig. 6 Comparison of the resulting modulation signals of example 1, with $m_{a,1} = 1, m_{a,3} = 0$ and $\varphi_3 = 0^\circ$, based on **a** carrier-based PWM with addition of a zero-sequence signal and **b** on the SVPWM algorithm [18] from Sect. 5.2

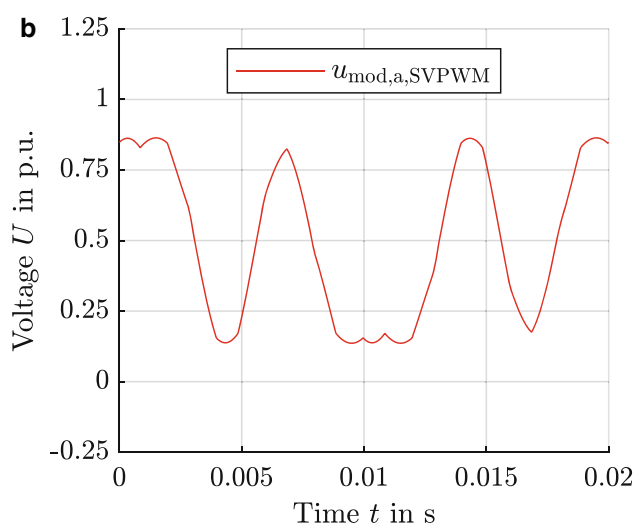
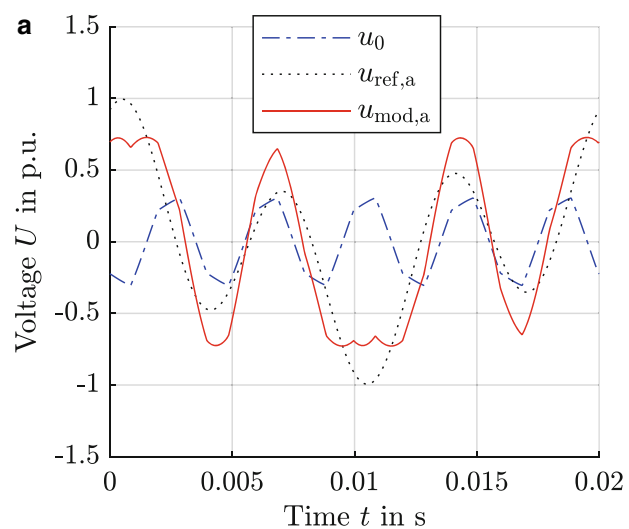


Fig. 7 As Fig. 6 but for $m_{a,1} = 0.4$, $m_{a,3} = 0.6$ and $\varphi_3 = 30^\circ$ (example 2)

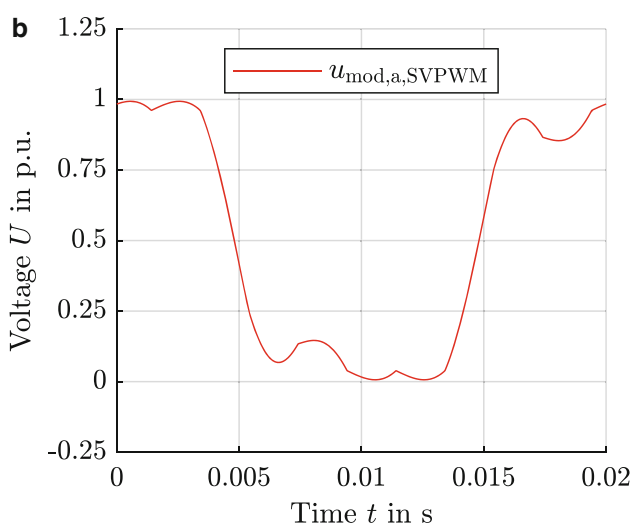
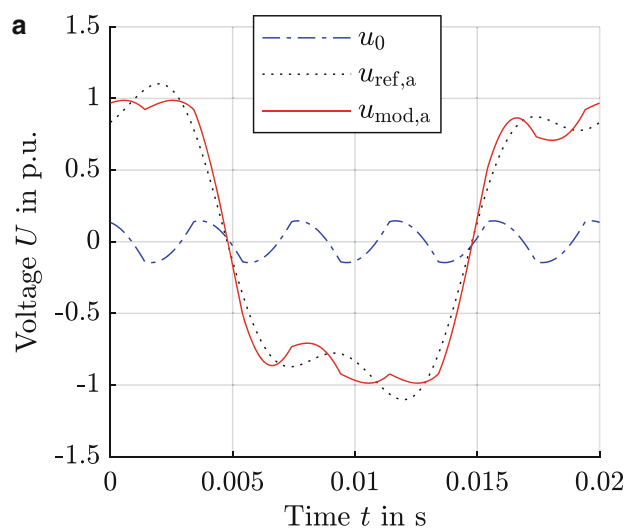


Fig. 8 As Fig. 6 but for $m_{a,1} = 1.1$, $m_{a,3} = 0.3$ and $\varphi_3 = 153^\circ$ (example 3)

r FFT spectra with mainly the 5th and 15th harmonics appearing. The main difference are the amplitudes $|u_0(n)|$ and phase-shifts of the harmonic components. Thus, the zero-sequence signals from all three examples 1, 2 and 3 satisfy the condition of only containing harmonics which are a multiple of five. It is confirmed that the application of the signal (7) is also valid for an arbitrary injection of a 3rd harmonic component and equivalent to the SVPWM algorithm of [18].

7 Conclusion

The carrier-based PWM method for three-phase systems based on the addition of a triangle zero-sequence signal with three times the fundamental frequency to the reference signal, is successfully adapted to a five-phase system. It is known from [9, 16] that this adaptation works for the injection of a pure sinusoidal fundamental component. This work expands

this concept showing that the addition of the non-sinusoidal zero-sequence signal with five times the fundamental frequency works for five-phase systems to inject arbitrary fundamental and 3rd harmonic components at the same time. To do this, a five-phase SVPWM algorithm from [18] was studied. This algorithm allows a broader spectrum of permissible combinations of fundamental and 3rd harmonic components than the well-established SVPWM algorithm, based on selecting neighbouring space vectors [12]. Instead of the time-consuming SVPWM algorithm [18], the addition of a non-sinusoidal zero-sequence signal is considered, which is more suitable for real-time applications. It is also favoured in order to avoid an increased data storage via look-up tables. The SVPWM algorithm of [18] was coded in *MATLAB* in order to generate the modulation signals for comparison with the method implementing the non-sinusoidal zero-sequence signal, proving the identical

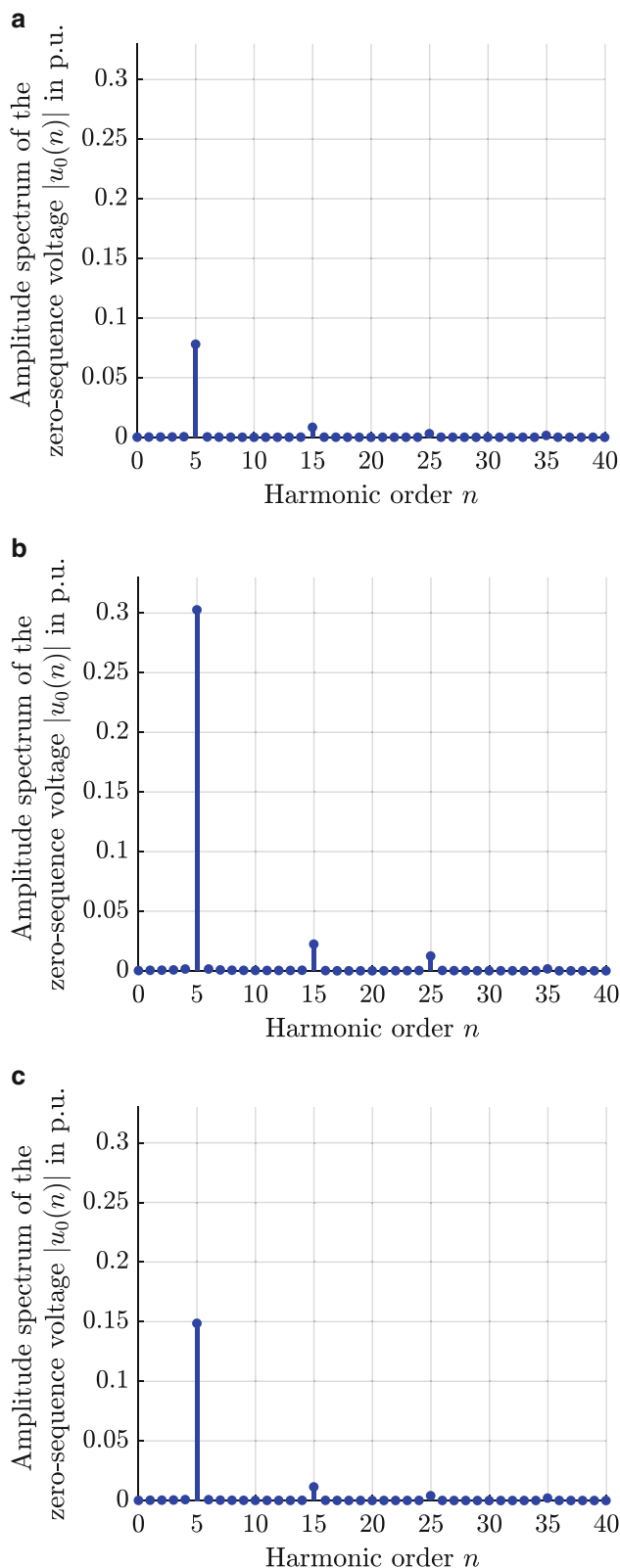


Fig. 9 FFT analysis of the resulting zero-sequence signals u_0 for **a** example 1: $m_{a,1} = 1$, $m_{a,3} = 0$, $\varphi_3 = 0^\circ$ **b** example 2: $m_{a,1} = 0.4$, $m_{a,3} = 0.6$, $\varphi_3 = 30^\circ$ and **(3)** example 3: $m_{a,1} = 1.1$, $m_{a,3} = 0.3$, $\varphi_3 = 153^\circ$

results of both methods, with three examples from the region of possible combinations of fundamental and 3rd harmonic components. Finally, an FFT analysis was performed on the resulting zero-sequence signals to prove that these still fulfill the conditions of containing only harmonics which are multiples of five.

Acknowledgements This Project is funded by the Deutsche Forschungsgemeinschaft (DFG, German Research Foundation) – DFG project Nr. 512518457.

Funding Open Access funding enabled and organized by Projekt DEAL.

Open Access This article is licensed under a Creative Commons Attribution 4.0 International License, which permits use, sharing, adaptation, distribution and reproduction in any medium or format, as long as you give appropriate credit to the original author(s) and the source, provide a link to the Creative Commons licence, and indicate if changes were made. The images or other third party material in this article are included in the article's Creative Commons licence, unless indicated otherwise in a credit line to the material. If material is not included in the article's Creative Commons licence and your intended use is not permitted by statutory regulation or exceeds the permitted use, you will need to obtain permission directly from the copyright holder. To view a copy of this licence, visit <http://creativecommons.org/licenses/by/4.0/>.

References

1. Singh G (2002) Multi-phase induction machine drive research—a survey. *Electr Power Syst Res* 61(2):139–147
2. Levi E (2008) Multiphase electric machines for variable-speed applications. *IEEE Trans Ind Electron* 55(5):1893–1909
3. Shah B, Rangari S, Renge M (2016) Analytical and comparative study of FHI-SPWM and SPWM control technique of Five-phase VSI. In: *International Conference on Power Electronics, Intelligent Control and Energy Systems (ICPE-ICES) Delhi*, pp 1–6
4. Iqbal A, Levi E, Jones M, Vukosavic SN (2006) Generalised sinusoidal PWM with harmonic injection for multi-phase VSIs. In: *IEEE Power Electronics Specialists Conference Jeju, Korea*, pp 1–7
5. Chinmaya KA, Singh GK (2018) Modeling and Comparison of Space Vector PWM Schemes for a Five-Phase Induction Motor Drive. In: *Annual Conference of the IEEE Industrial Electronics Society (IECON) Washington, DC*, pp 559–564
6. Toliyat H, Shi R, Xu H (2000) A DSP-based vector control of five-phase synchronous reluctance motor. In: *Conference on Industrial Applications of Electrical Energy (IAS) Rome*. vol 3, pp 1759–1765
7. Levi E, Bojoi R, Profumo F, Toliyat H, Wil-liamson S (2007) Multiphase induction motor drives – A technology status review. *Electr Power Appl IET* 1:489–516
8. Prieto J, Jones M, Barrero F, Levi E, Toral S (2011) Comparative analysis of discontinuous and continuous PWM techniques in VSI-fed five-phase induction motor. *IEEE Trans Ind Electron* 58(12):5324–5335
9. Iqbal A, Moinuddin S (2009) Comprehensive relationship between carrier-based PWM and space vector PWM in a five-phase VSI. *IEEE Trans Power Electron* 24(10):2379–2390

10. Zhu P, Zhang X-F, Qiao M-Z, Cai W, Liang J-H (2012) Harmonics Injected SVPWM Method for Five-Phase H-Bridge Inverter. In: Asia-Pacific Power and Energy Engineering Conference Shanghai, pp 1–4
11. Yong C, Qiu-Liang H (2019) Four-dimensional space vector PWM strategy for five-phase voltage source inverter. IEEE Access 7:59 013–59 021
12. Iqbal A, Levi E (2005) Space vector modulation schemes for a five-phase voltage source inverter. In: European Conference on Power Electronics and Applications Dresden, pp 1–12
13. Ryu H-M, Kim J-H, Sul S-K (2005) Analysis of multiphase space vector pulse-width modulation based on multiple d-q spaces concept. IEEE Trans Power Electron 20(6):1364–1371
14. Durán MJ, Prieto J, Barrero F, Riveros JA, Guzman H (2013) Space-vector PWM with reduced common-mode voltage for five-phase induction motor drives. IEEE Trans Ind Electron 60(10):4159–4168
15. Jiang D, Qian W (2013) Study of five-phase space vector PWM considering third order harmonics. In: IEEE Energy Conversion Congress and Exposition Denver, pp 4227–4232
16. Dujic D, Jones M, Levi E (2007) Continuous Carrier-Based vs. Space Vector PWM for Five-Phase VSI. In: The International Conference on “Computer as a Tool” (EUROCON) Warsaw, pp 1772–1779
17. Holmes DG, Lipo TA (2003) Pulse width modulation for power converters (principles and practice). Jon Wiley & Sons
18. Duran MJ, Toral S, Barrero F, Levi E (2007) Real-time implementation of multi-dimensional five-phase space vector PWM using look-up table techniques. In: Annual Conference of the IEEE Industrial Electronics Society (IECON) Taipei, pp 1518–1523
19. Lewicki A, Strankowski P, Morawiec M, Guziński J (2017) Optimized Space Vector Modulation strategy for five phase voltage source inverter with third harmonic injection. In: European Conference on Power Electronics and Applications (ECCE) Warsaw, pp 1–10
20. Lega A, Mengoni M, Serra G, Tani A, Zarri L (2008) General theory of space vector modulation for five-phase inverters. In: IEEE International Symposium on Industrial Electronics Cambridge, pp 237–244
21. Duran MJ, Levi E (2006) Multi-dimensional approach to multi-phase space vector pulse width modulation. In: Annual Conference on IEEE Industrial Electronics (IECON) Paris, pp 2103–2108
22. Dujic D, Grandi G, Jones M, Levi E (2008) A space vector PWM scheme for multifrequency output voltage generation with multiphase voltage-source inverters. IEEE Trans Ind Electron 55(5):1943–1955
23. López O, Dujic D, Jones M, Freijedo FD, Doval-Gandoy J, Levi E (2011) Multidimensional two-level multiphase space vector PWM algorithm and its comparison with multifrequency space vector PWM method. IEEE Trans Ind Electron 58(2): 465–475. <https://doi.org/10.1109/TIE.2010.2047826>
24. Kelly J, Strangas E, Miller J (2003) Multiphase space vector pulse width modulation. IEEE Trans Energy Convers 18(2):259–264
25. Hava A, Kerkman R, Lipo T (1999) Simple analytical and graphical methods for carrier-based PWM-VSI drives. In: IEEE transactions on power electronics, pp 49–61

Publisher's Note Springer Nature remains neutral with regard to jurisdictional claims in published maps and institutional affiliations.



Marc Ramos Friedmann, M.Sc. Mechatronics (Mechatronic Drives), Technical University Darmstadt in 2023. B.Sc. Mechatronics, Technical University of Darmstadt in 2021.



Alexander Möller, M.Sc. Electrical Engineering, Technical University Darmstadt in 2019; since 2019 research assistant at the Institute for Electrical Energy Conversion, TU Darmstadt; field of research: comparison of three- and five-phase squirrel cage induction machines and permanent magnet synchronous machines.



Andreas Binder, Prof. Dr.-Ing. habil. Dr. h.c., Diploma and doctoral degree in electrical engineering, Vienna University of Technology, Austria; 1981 to 1983 ELIN-Union AG, Vienna, development engineer; 1983 to 1989 researcher at the Institute of Electrical Machines and Drives, Vienna University of Technology; 1989 to 1997 Siemens AG, Bad Neustadt and Erlangen, group leader in motor and drive development; from 1997 to 2023 Head of the Institute of Electrical Energy Conversion, Technical University of Darmstadt, as full professor; 2007 Medal of Honor of the ETG/VDE; Senior Member IEEE, member VDE, IET, VDI, EPE.